

<https://doi.org/10.1038/s43856-025-00810-0>

Individualized cerebellar damage predicts the presence of behavioral disorders in children with brainstem tumors

Check for updates

Heyuan Jia^{1,2}, Kaikai Wang³, Mingxin Zhang⁴, Guocan Gu⁴, Yiyi Mai⁴, Xia Wu³, Congying Chu³, Xuntao Yin⁵, Peng Zhang⁴✉, Lingzhong Fan^{3,6}✉ & Liwei Zhang^{4,7,8}✉

Abstract

Background Brainstem tumors often cause intractable neurobehavioral issues, which can be a challenge for patients and surgeons. Research on cerebellar changes in these patients is limited, despite symptoms similar to cerebellar injuries. This study aims to investigate cerebellar damage pattern resulting from brainstem tumors and its association with behavioral disorders.

Methods This study enrolled 147 children with brainstem tumors. A U-Net-based segmentation algorithm is used to divide their cerebellums into 26 lobules. And these lobules are then used to build a normative model for assessing individual structural deviations. Furthermore, a behavior prediction model is developed using the total outlier count (tOC) index and cerebellar lobule volume as predictive features.

Results Over 95% of patients are found to have negative deviations in cerebellar regions, particularly in anterior lobules like Left V. Higher tOC is significantly associated with severe social problems ($r = 0.31$, $p = 0.001$) and withdrawal behavior ($r = 0.28$, $p = 0.001$). Smaller size of cerebellar regions strongly correlates with more pronounced social problems ($r = 0.27$, $p = 0.007$) and withdrawal behavior ($r = 0.25$, $p = 0.015$). Notably, lobules Right X, V, IV, VIIIB, Left IX, VIII, and X influence social problems, while Left V, Right IV, Vermis VI, and VIII impact withdrawal behavior.

Conclusions Our study reveals cerebellar damage patterns in patients with brainstem tumors, emphasizing the role of both anterior and posterior cerebellar lobes in social problems and withdrawal behavior. This research sheds light on the cerebro-brainstem-cerebellar underlying complex behavioral disorders in brainstem tumor patients.

Plain language summary

The cerebellum is an important brain region that is associated with motor control and cognitive function. Brainstem tumors, which are located near the cerebellum, have been shown to impact cerebellum function. However, the extent of this impact and its association with behavioral disorders remain unclear. This study uses data from healthy children to develop a behavioral prediction model based on changes in the size of specific regions within the cerebellum using artificial intelligence. When applied to children with brainstem tumors, the results reveal that the anterior region of the cerebellum is most severely damaged. Additionally, overall cerebellar damage, especially in the posterior region of the cerebellum, is linked to social problems and withdrawal behaviors. This study highlights the model's ability to assess brain structural changes and its potential to predict behavioral disorders based on the location of the cerebellum damage in patients with brainstem tumors.

Brainstem tumors originate in the medulla oblongata, pons, and midbrain, making up 15% of pediatric brain tumors. Diffuse intrinsic pontine gliomas (DIPG) account for 80% of these cases and are associated with a poor prognosis and complex neurological dysfunction¹. Historically, higher cognitive functions were not attributed to the brainstem². However, recent reports show abnormal cognitive and behavioral disorders in patients with

brainstem lesions, which are often masked by severe neurological symptoms³. Notably, symptoms like behavioral disorders, attention deficits, social disturbances, irritability, and flattened affect are now gaining clinical attention. These issues can persist long after surgery⁴. Recent neuropsychological research demonstrates widespread behavioral impairments in children with brainstem tumors⁵, aligns with previous findings in

¹School of Instrumentation and Optoelectronic Engineering, Beihang University, Beijing, China. ²Institute of Large-scale Scientific Facility and Centre for Zero Magnetic Field Science, Beihang University, Hangzhou, China. ³Brainnetome Center, Institute of Automation, Chinese Academy of Sciences, Beijing, China. ⁴Department of Neurosurgery, Beijing Tiantan Hospital, Capital Medical University, Beijing, China. ⁵Department of Radiology, Guangzhou Women and Children's Medical Center, Guangzhou Medical University, Guangzhou, China. ⁶School of Health and Life Sciences, University of Health and Rehabilitation Sciences, Qingdao, China. ⁷China National Clinical Research Center for Neurological Diseases, Beijing Tiantan Hospital, Capital Medical University, Beijing, China. ⁸Beijing Neurosurgical Institute, Beijing Tiantan Hospital, Capital Medical University, Beijing, China. ✉e-mail: zhang_roc@163.com; lingzhong.fan@ia.ac.cn; zhangliwei@163.com

posterior fossa tumors⁶. Researchers believe these behaviors may result from cerebellar damage⁷. However, systematic investigations into indirect cerebellar changes and their impact on cognitive functions in brainstem tumor patients are still limited.

The cerebellum, located beneath and behind the cerebral cortex, is closely connected to the brainstem via dense neural fiber bundles⁸. The corticospinal tract and spinocerebellar tract connect cortical brain regions with the contralateral cerebellum through the intermediary pontine region⁹. Additionally, fascicular pontocerebellar fibers extend extensively into the opposite hemisphere, forming crucial cerebellar peduncles¹⁰. Moreover, the cerebellum also connects with the hypothalamus, limbic system, and various brainstem regions such as the ventral tegmental area¹¹. The close spatial relationship predisposes the growth of brainstem tumors to potentially the normal functioning of the cerebellum¹². Current research suggests that the brainstem engages in cognitive processing through its interaction with the frontal lobe system and also plays a role in cognitive processing as an integral part of the cerebro-cerebellar circuit¹³. Clinical observations support the hypothesis, showing that ipsilateral cerebellar atrophy is common in brainstem tumor cases, as well as in brainstem ischemia, stroke, and trauma¹⁴. This may be due to damage to the direct fiber connections between the brainstem and cerebellum¹⁵.

In recent years, research has primarily focused on the non-motor functions of the cerebellum. The anterior regions of the cerebellum, including lobules I-IV and lobule VIII, are mainly associated with motor functions, while the posterior and lateral regions are closely linked to non-motor functions¹⁶. Some functional imaging studies have shown that various cognitive tasks can activate the posterior cerebellum. For instance, during social cognitive tasks, regions such as Crus I and II in the posterior cerebellum are significantly activated, indicating its crucial role in social understanding and learning sequences of social behavior¹⁷. Schmahmann identified the cerebellar cognitive affective syndrome (CCAS), resulting from posterior cerebellar damage. It is characterized by executive dysfunction, spatial cognitive impairments, language disorders, and changes in personality and emotion¹⁰. Notably, the impairments caused by these damages are similar to the symptoms caused by brainstem tumors¹⁸. Thus, we hypothesize that the complex behavioral disorders observed in patients are caused by heterogeneous alterations in the cerebellum resulting from brainstem tumors.

To test our hypothesis, we employed the ACAPULCO (Automatic Cerebellum Anatomical Parcellation using U-Net with Locally Constrained Optimization) for effective cerebellar segmentation of deformed cerebellum. Additionally, we established a normative model to quantify cerebellar damage pattern by integrating data from healthy children. This model allowed us to assess individual deviations in brainstem tumor patients. Subsequently, we used machine learning to link these deviations to specific behaviors, identifying cerebellar regions associated with each behavior. Through these investigations, we sought to uncover the underlying brain mechanisms responsible for behavioral impairments in patients with brainstem tumors. Ultimately, the study identifies widespread cerebellar structural abnormalities in over 95% of patients, with the most pronounced negative deviations observed in anterior lobules. Higher total outlier counts (tOC) values are linked to severe social dysfunction and withdrawal behavior. Reduced cerebellar volume further exacerbates these behavioral deficits.

Methods

Participants

A cohort of 171 pediatric patients (age range: 4–17 years) diagnosed with brainstem tumors at the Department of Neurosurgery, Beijing Tiantan Hospital, were enrolled between April 2019 and December 2022. Inclusion criteria were as follows: 1) Initial diagnosis of brainstem tumor with no prior treatment, including chemotherapy, radiotherapy, or other interventions; 2) Tumors confined to the brainstem without infiltrating the cerebellum, spinal cord, or thalamus; 3) Absence of comorbid psycho-neurological disorders, behavioral and personality disorders; 4) No history of developmental disorders. All patients underwent 3DT1 magnetic resonance

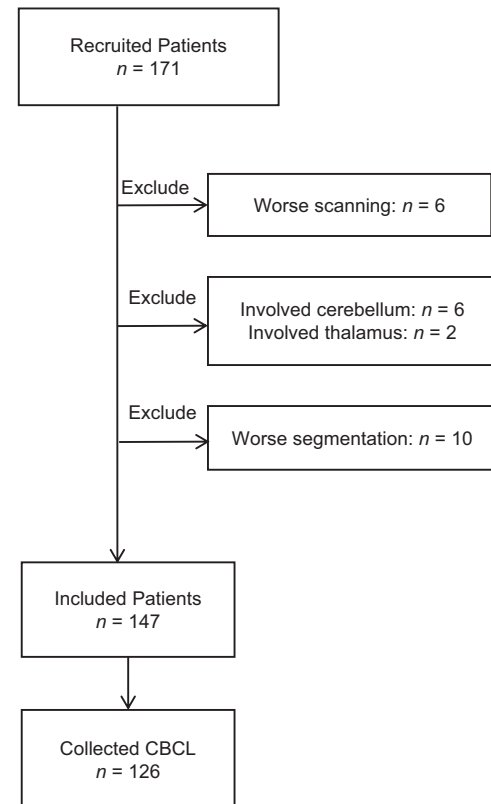


Fig. 1 | The flow chart of patient enrollment. 171 patients were recruited initially. Subsequently, individuals with poor scanning quality, tumor involvement of the cerebellum or thalamus, and suboptimal segmentation were removed. After these removals, 147 patients were included in the final analysis. Among the 147 enrolled patients, 126 completed the Child Behavior Checklist (CBCL).

imaging (MRI) during their initial visit and completed the Child Behavior Checklist (CBCL) scale - Parent version.

To establish a normative model, data from 849 healthy children (age range: 4–18 years) were collected from publicly available databases, including 72 locally recruited children in Beijing (61 of whom underwent scanning), 69 from the fcon_1000.projects dataset (https://doi.org/10.15387/fcp_indi.corr.ipcas7)¹⁹, 450 from the Child Connectome Project (CCNP)²⁰, and 269 from the Children's Hospital in Guangzhou. After excluding subjects with severe cerebellar compression or poor image quality, our final analysis included 147 patients and 849 healthy children. Figure 1 illustrates the enrollment process in a flowchart. We downloaded MRI T1 images and corresponding phenotypic information from these databases, with the demographic characteristics of the subjects summarized together. All procedures performed in studies involving human participants were approved by the Institutional Review Board (IRB) of Beijing Tiantan Hospital, Capital Medical University (Approval No. KY 2019-124-02) and conducted in accordance with the 1964 Helsinki Declaration and its later amendments or comparable ethical standards. Informed consent was obtained from all participants' parents prior to study enrollment, with written documentation adhering to the requirements of the IRB.

We confirm that this study does not involve the export of human genetic materials or data from China. All original brain MRI data and phenotypic data were collected, processed, and stored within China. The data provided in this study are derived from de-identified brain image processing and do not contain raw imaging data or individually identifiable information. Specifically: (1) Raw MRI data were processed using standardized pipelines in China, with no transfer of original images to foreign institutions. (2) Derived variables (e.g., regional volume, clinical characteristics) were anonymized and aggregated to ensure no re-identification of participants. (3) All analyses were performed on servers located in China.

(4) The data of healthy children were sourced from publicly accessible databases, such as devCNNP. These databases do not include any Chinese human genetic resources. This study fully complies with the “Guidance of the Ministry of Science and Technology (MOST) for the Review and Approval of Human Genetic Resources” and the ethical standards of Beijing Tiantan Hospital’s Institutional Review Board (Approval No. KY 2019-124-02).

MRI acquisition and processing

Structural MRI scans were performed using a 3.0 T scanner (Ingenia CX, Philips Healthcare) with a 32-channel head receiver coil. The 3D T1-weighted sequence included 196 contiguous sagittal slices with a voxel size of $1.0 \times 1.0 \times 1.0 \text{ mm}^3$ (TR = 6.572 ms; TE = 3.025 ms; FA = 8°). DICOM images were converted to NIFTI format. Figure 2 shows the 3D T1-weighted imaging features of MRI in axial, coronal and sagittal planes, respectively, with tumors located in the medulla oblongata (Fig. 2A), pons (Fig. 2B) and midbrain (Fig. 2C). Figure S1 illustrates the cerebellar segmentation workflow. First, the brainstem was excluded to avoid misclassification by delineating it as the volume of interest (VOI) using MRICroGL. Next, preprocessed MRI data from patients, along with data from healthy children, were then processed using the ACAPULCO package (version 0.2.1) with a pediatric template to generate segmented cerebellar images. ACAPULCO demonstrated high segmentation accuracy with superior mean Dice scores across multiple regions, excellent reproducibility, fast computational speed, and broad applicability across various datasets and disease types²¹. Following this, segmentation quality

was independently inspected by two neurosurgery specialists. Each specialist conducted their review separately, and manual corrections were performed for inaccurately segmented images based on cerebellar lobule anatomical morphology using ITK-SNAP. Afterward, the two specialists discussed their findings to finalize the most accurate segmentation. Ultimately, we obtained volumes for 28 cerebellar regions, including left and right lobules I-III, IV, V, VI, VII, VIIIA, VIIIB, IX, X, Crus I, Crus II, and vermis lobules VI, VII, VIII, IX, X, and corpus medullare. Due to inconsistent boundaries between lobules VIIIA and VIIIB, these regions were merged into single lobules VIII for the left and right sides, respectively. This workflow ultimately yielded volume measurements for 26 cerebellar lobules, which were analyzed for their associations with behavioral outcomes.

Behavioral assessment

Participants’ behavioral profiles were assessed using the Achenbach Child Behavioral Checklist (CBCL), comprising 113 items categorizing behavioral issues into eight factors: somatic complaints, withdrawal behaviors, depression/anxiety, aggressive behaviors, delinquent behavior, thought problems, and social problems²².

Data harmonization

We utilized the Combat method to harmonize data from different sources, mitigating non-biological variance from inter-scanner discrepancies. This method has been validated for effectively reducing unwanted variation introduced by site differences in structure MRI investigations²³. Notably,

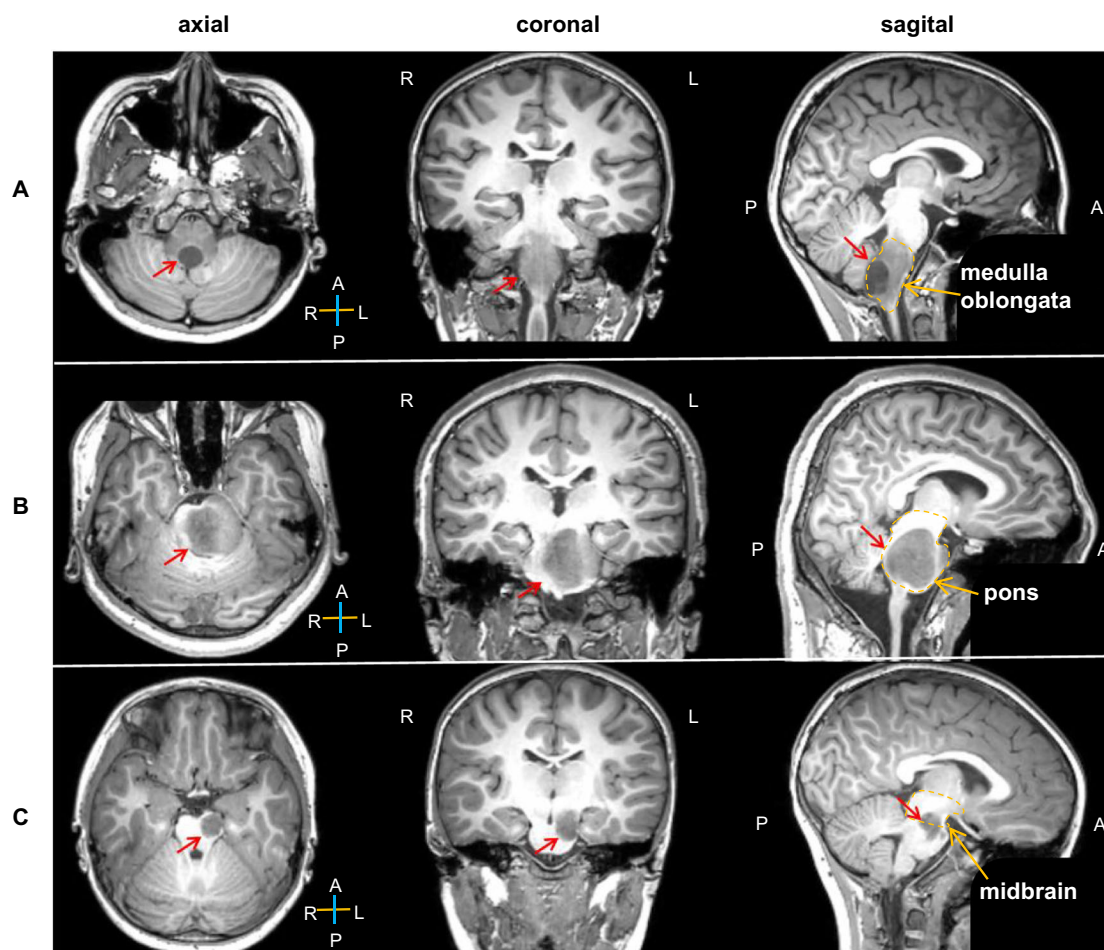


Fig. 2 | The radiological characteristics of patients with brainstem tumors. The 3D-T1 weighted MRI images show the imaging in axial, coronal, and sagittal positions of the primary tumors located in the medulla oblongata (A), pons (B), and

midbrain (C). The red arrow highlights the tumor tissue, characterized by an uneven low signal. The yellow contoured regions, arranged from top to bottom, correspond to the medulla oblongata, pons, and midbrain regions, respectively.

this method retained age, gender, and TIV as covariates while excluding diagnostic labels.

Normative modeling

Using volumetric data from the 26 cerebellar regions, we established normative models with Gaussian Process Regression (GPR), incorporating age and gender as covariates²⁴. This Bayesian non-parametric modeling approach inherently considers prediction uncertainty and provides probability distributions for predicted values. We initially estimated models with 10-fold cross-validation on the healthy children dataset, then developed definitive models for deviation analysis in patients. For each participant, the normative model was used to predict volume estimates for each region, along with corresponding predictive uncertainty. Predictive uncertainty contours were then used to characterize centile variations within the cohort, enabling us to parameterize volume deviations relative to the reference cohort.

Estimation of cerebellar volume deviations for each subject

For each glioma patient, we utilized normative percentile charts from healthy children to assess individual deviations in cerebellar region volumes. Deviations were quantified by computing a Z-score based on observed and predicted volume values for each region. For each patient i , the Z score of a cerebellum region j was calculated using the formula:

$$Z_{ij} = \frac{y_{ij} - \hat{y}_{ij}}{\sqrt{\sigma_{ij}^2 + \sigma_{nj}^2}} \quad (1)$$

where y_{ij} is the true volume value, \hat{y}_{ij} is the expected volume value estimated from the GPR, σ_{ij} is the predictive uncertainty, and σ_{nj} is the variance learned from the normative distribution n .

Statistics and Reproducibility

The relative deviation distribution for each patient was compared to the general norm using the normative model. The deviation rate was computed by counting patients with Z-values exceeding ± 1.96 and dividing by the total patient count. This yielded positive and negative deviation rates, indicating the extent of deviations in each brain region. Outliers with diminished cerebellar volume (< -1.96 , below the 2.5th percentile of the normative distribution) were identified in each region. We focused on this lower threshold to assess volume reductions linked to tumors. The tOC across all 26 regions was calculated for each participant²⁵.

Pearson correlation analysis investigated associations between tOC and clinical symptoms, especially social problems and withdrawal behaviors. A ridge regression model with nested fivefold cross-validation (5F-CV) evaluated tOC's predictive power for essential behaviors. The outer loop assessed the model's generalization to unseen subjects, and the inner loop performed a grid search to identify the optimal parameter within a specified λ range ($[2^{-10}, 2^{-9}, \dots, 2^4, 2^5]$). We conducted 101 repetitions of the 5F-CV, calculating prediction accuracy as the mean r value of the five folds, resulting in a final accuracy of the median r value from 101 replicates. Linear regression was applied within each fold to adjust for age and sex effects. Permutation testing assessed the prediction's significance by estimating the empirical distribution of prediction accuracy under the null hypothesis of no association between cerebellar volume deviations and behavior values. The prediction procedure was repeated 1000 times to create the null distribution. In each iteration, behavior scores were permuted across the training samples²⁶.

To evaluate whether cerebellar volume deviations captured significant behavioral traits, we combined scores from 26 regions into a feature vector for each individual and adjusted the ridge regression model accordingly. Feature weights indicated each region's importance and its positive or negative association with behavior. We evaluated these weights across 101 iterations, focusing on the median r value. Significance was determined through 1000 permutation tests, where positive weights indicated larger volumes linked to higher behavioral scores, and negative weights indicated smaller volumes associated with higher scores.

Clinical data were collected at the time of patient initial visits, including clinical symptoms, disease duration, and Karnofsky Performance Status (KPS) scores. We also diagnosed whether the patient had Diffuse Intrinsic Pontine Glioma (DIPG) and used MRICron software to manually delineate the tumor regions for tumor volume calculation. Subsequently, we applied multiple linear regression models to explore the associations between these clinical variables and tOC values. A two-tailed p -value threshold of 0.05 was used for statistical significance.

A normative model was built using GPR regression on data from healthy children. For the behavioral prediction model, a separate sample of 126 patients was used with Ridge regression. The model's performance was evaluated using 10-fold cross-validation, and statistical significance was assessed through 1000 permutation tests. All analyses were conducted in Python (version 3.7). Supplementary case-control behavioral analysis included 126 patients and 72 healthy children, achieving sufficient power ($d = 0.5$, $\alpha = 0.05$, power = 0.8) for detecting medium-sized effects with balanced sample sizes.

Reporting summary

Further information on research design is available in the Nature Portfolio Reporting Summary linked to this article.

Table 1 | The demographic of cohorts and clinical characteristics

Characteristics	Patients ($n = 147$)	Healthy children ($n = 849$)
Demographics		
Age, years	8.5 ± 3.5	11.44 ± 3.3
Sex, n (%)		
Male	77 (52.4%)	477 (56.2%)
Female	70 (47.6%)	372 (43.8%)
Clinical parameters		
KPS, points	77 ± 10	NA
Duration, months	5.4 ± 11.2	NA
Tumor volume, cm^3	26.97 ± 14.7	NA
tOC, number	1.3 ± 2.0	NA
Symptom, n (%)		
Headache	42 (28.6%)	NA
Emesis	42 (28.6%)	NA
Diplopia	80 (54.4%)	NA
Bucking	66 (44.9%)	NA
Dysphagia	24 (16.3%)	NA
Dysarthria	37 (25.2%)	NA
Limb weakness	85 (57.8%)	NA
Ataxia	82 (55.8%)	NA
Tumor location, n (%)		
Midbrain	12 (8.2%)	NA
Pons	92 (62.6%)	NA
Medulla	13 (8.8%)	NA
Multi-locations	30 (20.4%)	NA
DIPG diagnosis, n (%)		
Yes	116 (78.8%)	NA
No	31 (21.2%)	NA

Continuous variables are presented as mean \pm SD. Categorical variables are reported as counts (percentages). KPS Karnofsky Performance Status, SD standard deviation, tOC The total outlier count, DIPG Diffuse Intrinsic Pontine Glioma, NA Not applicable. Diagnosis standard of DIPG: characteristic MRI findings of diffuse pontine involvement with minimal contrast enhancement. Tumor volume was calculated by manually outlining the tumor and summing the voxel values. Multi-locations refers to tumors that involve more than two brainstem regions.

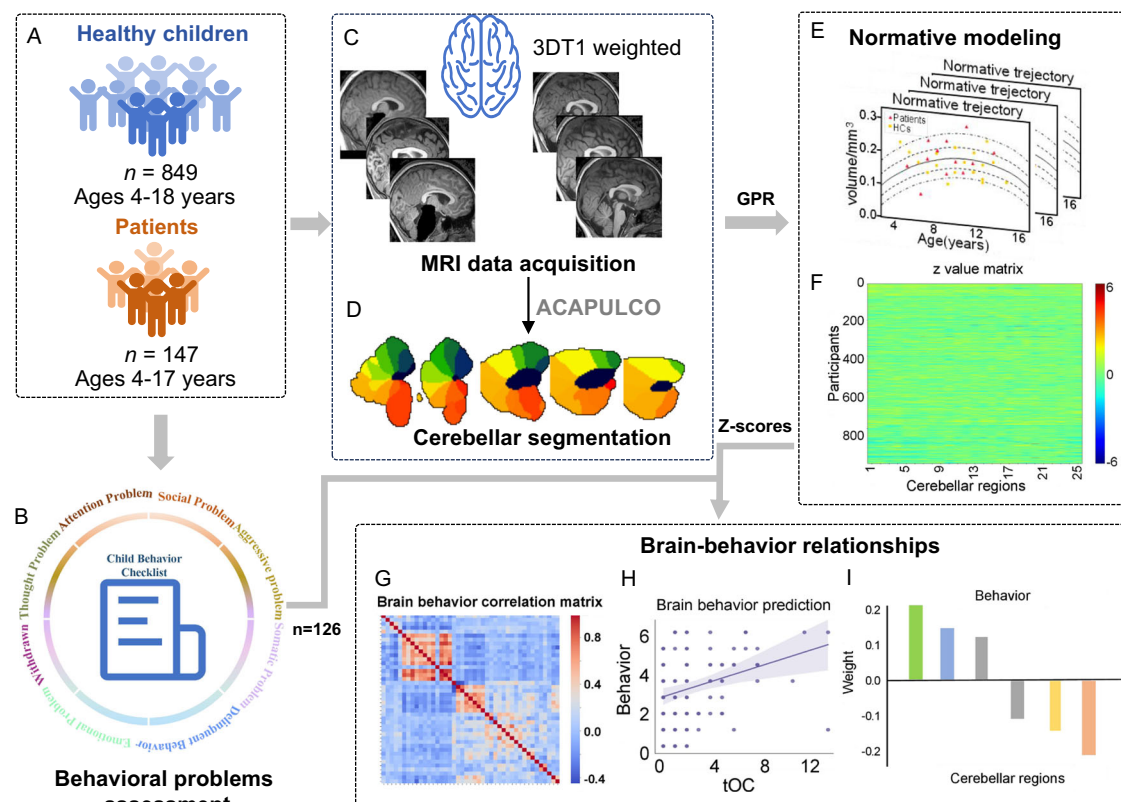


Fig. 3 | Data analysis flowchart. **A** Patient and multi-site healthy children enrolled. **B** Patients' behaviors were assessed in the neurosurgical clinic using the Child Behavior Checklist. **C** Structural MRI (T1) data acquisition and processing. Patients' brainstem was excluded before segmentation. **D** All participants' 28 cerebellar regions were obtained by Automatic Cerebellum Anatomical Parcellation using U-Net with Locally Constrained Optimization. **E** Normative trajectory in the GPR

Model. In each model, a Gaussian model of the volume of each brain region was established with age and sex as covariates. **F** The Z-score profile of individual cerebellar regions' volume. **G** Pearson correlation matrix of cerebellar regions and behavioral problems. **H** The deviations of cerebellar volume predict behaviors. **I** Feature weight maps for 26 cerebellar regions. GPR Gaussian Process Regression.

Results

Demographics of the cohort and clinical characteristics

Initially, we enrolled 171 pediatric patients diagnosed with brainstem tumors and 849 typically developing children from 4 different sites. After excluding cases with poor MRI scanning (6 patients, 8 healthy children), those with tumors involving the cerebellum or thalamus (6 patients), and those with segmentation issues (10 patients), our final analysis comprised 147 patients, with a mean age of 8.5 years and 77 males. Among these patients, the average KPS score was 77, with a mean symptom duration of 5.4 months (SD = 11.2). The most common symptoms at presentation were limb weakness (57.82%), ataxia (55.78%), and diplopia (54.42%). Other symptoms, such as headache (28.57%), emesis (28.57%), bucking (44.90%), dysphagia (16.33%) and dysarthria (25.17%), had lower incidence rates. Radiological findings showed that the majority of tumors were located in the pons (62.59%), followed by multiple brainstem locations (20.41%), the medulla (8.84%), and the mid-brain (8.16%). A total of 78.8% of patients were diagnosed with DIPG (Diffuse Intrinsic Pontine Glioma). The mean tumor volume was 26.97 cm³ (SD = 14.68 cm³). And the average total number of tOC was 1.3 (SD = 2.0). Besides, we constructed a normative model using data from 849 typically developing children, with a mean age of 11.44 years old and 477 males (see Table 1). Figure 3 shows the flow chart of the whole experiment.

Individual deviations of cerebellar volumes in patients

The normative trajectory derived from the GPR model for four cerebellar regions with the most extreme deviation demonstrated that patients' abnormal deviation values primarily fell below the lower boundary of the general norm (Fig. 4A). The violin chart indicates that the majority of both patients and healthy children exhibited zero extreme positive deviations, with only 2.5% of

subjects showing such deviations. In healthy children, tOC values were minimal and tightly clustered around zero. In contrast, patients exhibited a broader distribution of tOC values, with 95% of cases ranging between 3 and 10. Female patients exhibited a higher prevalence of extreme negative deviations compared to males (Fig. 4B). The stacked histogram suggested that patients primarily displayed positive deviations in the corpus medullare, while negative deviations were predominantly observed in Left I-III, Left V, Right V, Right I-III, Right X, Left X, Left IV, Vermis VI, Right IV, Vermis VII, and Right VIII (Fig. 4C). To investigate regional differences in cerebellar volume, we analyzed spatial distribution maps of extreme negative deviations (deviation rate > 0.2). As shown in Fig. 4D, negative deviations are predominantly concentrated in the anterior and posterior regions of the cerebellum.

Relationships between clinical features and tOC

The multiple regression analysis evaluates the influences of various clinical factors on tOC (see Table 2). The model exhibited that tumor_volume shows a statistically significant positive association with tOC ($p < 0.0001$, 95%CI: 0.33–1.11, $t = 3.667$), indicating that larger tumor volumes are linked to higher tOC ($r = 0.41$, $p < 0.001$) (see Figure S2). Other clinical factors such as Duration, Headache, KPS, et al. showed no significance in tOC value. Additionally, the behavioral profiles and group comparison results show that most behavioral issues in brainstem tumor patients are significantly more pronounced than in healthy children (see Figure S3). This underscores the importance of studying behavioral disorders in brainstem tumor patients.

Outliers are associated with cognitive function

Table S1 presents the results of the multiple regression analysis between each behavioral variable and clinical characteristics. The results indicate that tOC

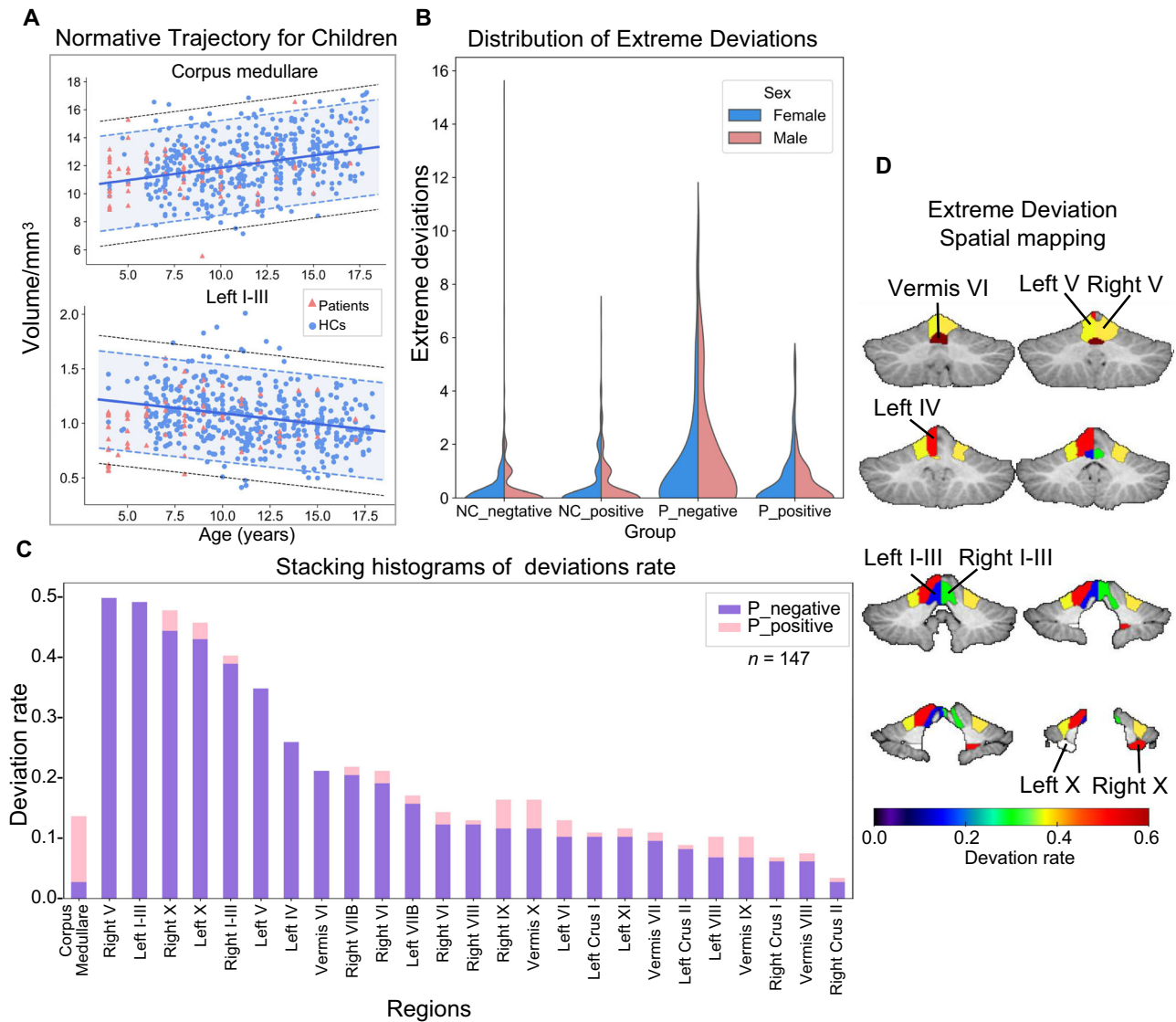


Fig. 4 | Normative model and the analysis of deviations. **A** The normative model was estimated using GPR. For the volume of 26 cerebellar lobes, the normative models were estimated. In each model, the volume of cerebellar regions was the response variable. Age and gender were covariates. Two subplots illustrate the normative developmental trajectories for the corpus medullare and left I-III in male patients and healthy children. Red triangles representing patients and blue dots

representing controls. **B** The violin plots display different distribution of positive and negative deviations in gender between patients and healthy children (HC).

C Stacking histograms of 26 cerebellar regions with positive and negative deviation rates in patients. The purple and pink bars represent negative and positive deviation, respectively. **D** Illustration of extreme negative deviation of cerebellar regions (deviation rate > 0.2). GPR Gaussian Process Regression.

is significantly associated with social problems ($p = 0.046$) and withdrawal behaviors ($p = 0.008$). Furthermore, our findings reveal a significant predictive relationship between the tOC and individuals' behavioral scores. Specifically, the analysis revealed a significant correlation between tOC and cognitive function, specifically with social problems ($r = 0.31$, $p = 0.001$) and withdrawal behaviors ($r = 0.28$, $p = 0.001$) as shown in Fig. 5A, B. Additionally, tOC was found to predict scores related to social problems (mean $r = 0.27$, $p = 0.030$) and withdrawal behaviors (mean $r = 0.25$, $p = 0.034$) as illustrated in Fig. 5C, D. These positive linear relationships indicate increased severity of social problems and withdrawal behaviors are associated with higher tOC values, which represent more severe cerebellar damage.

Predictive relationship between cerebellar volume deviations and behavior in glioma patients

Using the ridge regression model, we discovered a significant predictive association between cerebellar volume deviations and individuals' behavior scores. Specifically, our analysis revealed that cerebellar volume deviations

could predict scores associated with social problems ($r = 0.27$, $p = 0.007$) (Fig. 6A), and withdrawal behaviors ($r = 0.25$, $p = 0.015$) (Fig. 6B).

We observed that the region contribution weights predominantly displayed negative values, indicating reduced cerebellar volume in regions corresponding to more severe symptoms. For example, negative feature weights were evident in regions such as Right X, Right V, Right IV, Left IX, Left VIII, Left X, Left V, and Right VIIIB for social problems (Fig. 6C), and in regions like Left V, Right IV, Vermis VIII, Left X, Left IV, Left IX, Vermis VI, Right X, Right VIIIB, Vermis X, Right Crus I, and Right V for withdrawal behaviors (Fig. 6D). Furthermore, negative feature weights were consistent across both correlated behaviors in regions including Right X, Left X, Right V, Left V, Right IV, and Left IX.

Discussion

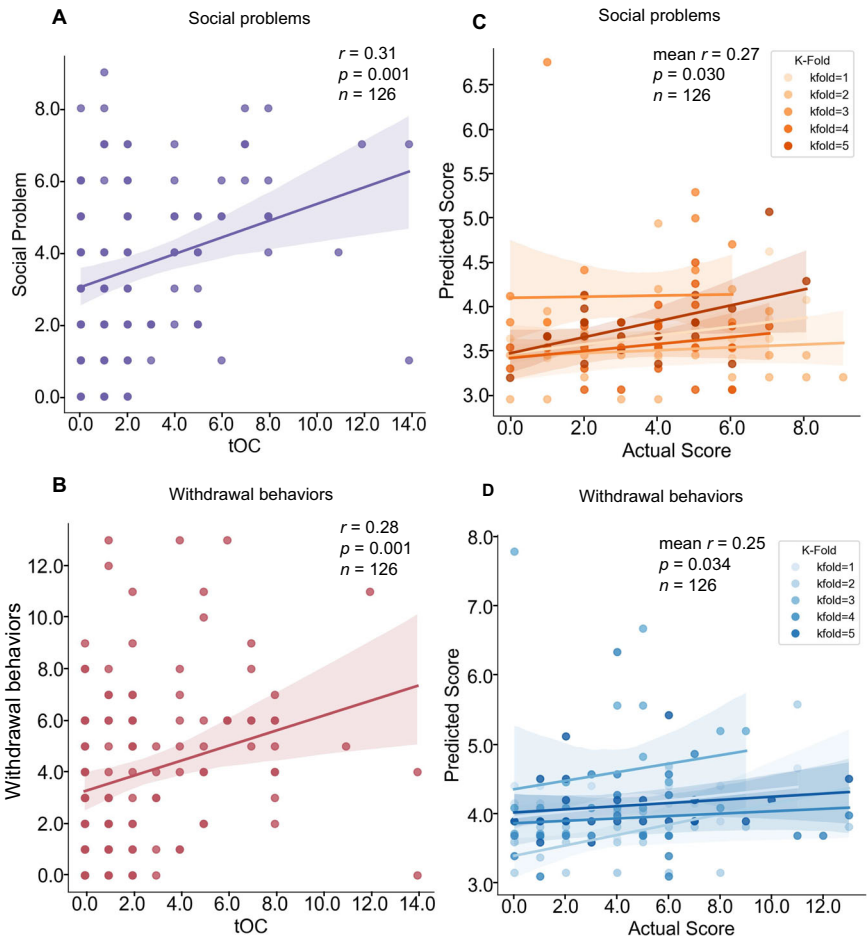
This investigation revealed a general reduction in cerebellar gray matter among patients diagnosed with brainstem tumors, demonstrating a heterogeneous pattern of atrophy. Significantly negative deviations were observed in Left I-V, Right I-V, and Vermis IV-VII. Additionally, a negative

Table 2 | Multiple Regression Analysis of Clinical Variables and association with tOC

Variables	Coef	SE	t	p > t	CI		VIF
					0.025	0.975	
Duration	0.1597	0.189	0.844	0.401	−0.215	0.535	1.137
Tumor_volume	0.7855	0.199	3.944	0.000	0.391	1.180	1.259
KPS	−0.0303	0.022	−1.375	0.172	−0.074	0.013	1.665
Location	0.168	0.2	0.842	0.402	−0.228	0.564	1.102
DIPG	−0.1078	0.504	−0.214	0.831	−1.107	0.892	1.403
Headache	0.1524	0.441	0.345	0.73	−0.722	1.027	1.202
Emesis	−0.2082	0.426	−0.489	0.626	−1.053	0.636	1.162
Diplopia	−0.1241	0.387	−0.32	0.749	−0.892	0.643	1.181
Bucking	−0.0418	0.4	−0.105	0.917	−0.834	0.750	1.260
Dysphagia	0.4861	0.557	0.872	0.385	−0.618	1.591	1.430
Dysarthria	−0.2161	0.479	−0.451	0.653	−1.166	0.734	1.389
Limb weakness	0.0245	0.413	0.059	0.953	−0.794	0.843	1.321
Ataxia	−0.1363	0.407	−0.335	0.738	−0.943	0.670	1.304

Coef coefficient, SE standard error, CI confidence interval, VIF variance inflation factor. The *p*-values in the table are two-tailed, with a threshold of 0.05 used to determine statistical significance, indicating whether each variable has a meaningful effect on the dependent variable.

Fig. 5 | Behavioral prediction models using individualized tOC. A, B Prediction of behaviors in glioma patients using ridge regression models based on tOC. Scatter plots show the relationship between tOC and social problems (A), as well as withdrawal behaviors (B). Each dot represents an individual sample, with observed behavioral scores plotted against tOC values. The solid line depicting the ridge regression fit and a shaded area indicating the 95% confidence interval. The Pearson correlation coefficient (*r*) quantifies the linear relationship between tOC and behavioral scores. Prediction of social problems (C) and withdrawal behaviors (D) in previously unseen individuals using tOC (total outlier count) with five-fold cross-validation. Points represent test samples (observed values on the x-axis; predicted values on the y-axis), with colors distinguishing folds. Lines depict fold-specific regression fits, and shaded areas indicate confidence intervals. Prediction accuracy is measured by the mean *r* across folds, with significant *p*-values for both behaviors. tOC the total outlier count.



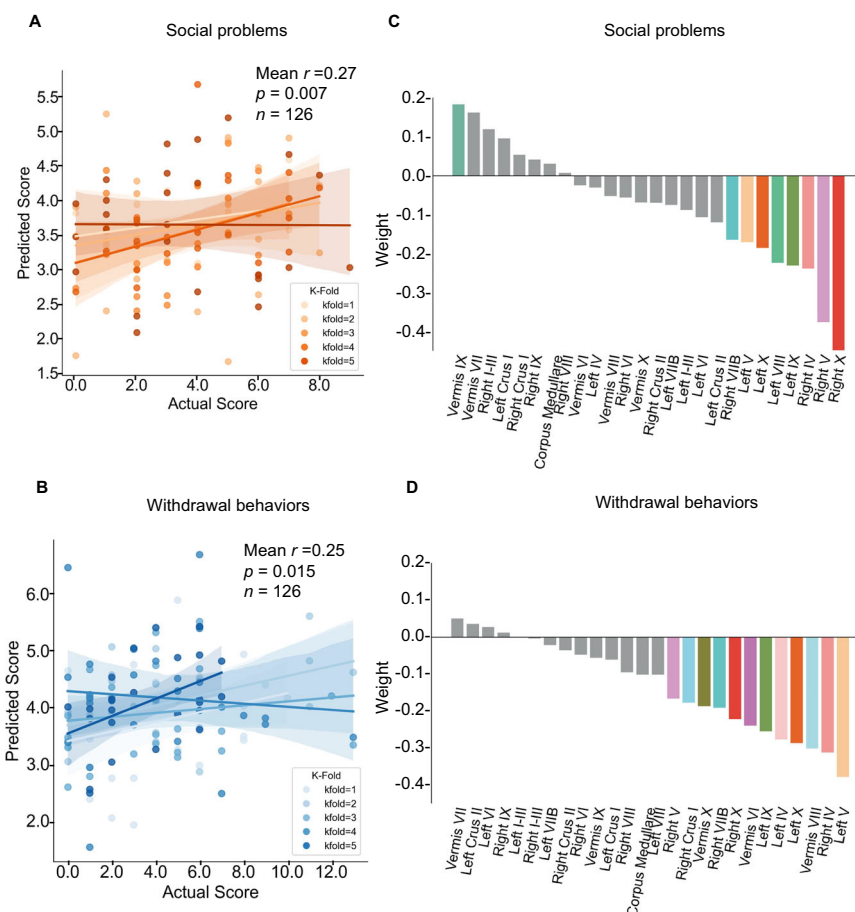
correlation was identified between cerebellar lobe deviation and both withdrawal behavior and social problems. Moreover, the total outlier score emerged as an individualized indicator of cerebellar damage, which is positively related to tumor volume. In summary, the aforementioned findings yield the following insights: 1) brainstem tumors disrupt the normal neuroanatomical development of the cerebellum, 2) behavioral issues in

children with brainstem tumors may be linked to abnormal cerebellar structures, 3) individual indicators of cerebellar lobular atrophy hold promise as predictors of behavioral outcomes. In the following sections, each of these findings will be further discussed.

Severe atrophy predominantly affects the anterior lobes and vermis cerebelli, with milder impacts on the posterior and lateral lobes. This

Fig. 6 | Behavioral prediction models of individual deviation of cerebellar volume. Scatter plots show the relationship between cerebellar volume deviation and behavioral scores for social problems (A) and withdrawal behaviors (B) using five-fold cross-validation. Points represent test samples, with colors distinguishing folds. Lines depict fold-specific regression fits, and shaded areas indicate confidence intervals. Prediction accuracy is measured by the mean Pearson correlation coefficient (r) across folds, with significant p -values for both behaviors.

C, D The feature weight maps for social problems and withdrawal behaviors highlight the contributions of specific brain regions to the predictions. For social problems (C), significant features include reduced cerebellar volume in regions such as Right X, Right V, Right IV, Left IX, Left VIII, Left X, Left V, and Right VIIIB, which primarily drive the prediction. For withdrawal behaviors (D), reduced cerebellar volume in regions such as Left V, Right IV, Vermis VII, Left X, Left IV, Left IX, Vermis VI, Right X, Right VIIIB, Vermis X, Right Crus I, and Right V are the key contributors. Features with non-significant *p*-values are represented by gray bars in both maps.



pattern likely arises primarily from compression due to the swollen brainstem. The current findings support clinical research highlighting the occurrence of secondary cerebellar atrophy induced by brainstem tumors. For example, previous studies reported significant cerebellar atrophy in patients with basal gangliocytoma involving the cerebellar peduncles¹⁴. Interestingly, cerebellar atrophy is common in patients with brainstem diseases. Recent research shows distinctive patterns of decreased cerebellar grey matter in patients with pontine infarctions, emphasizing lesion lateralization²⁷.

The cerebellum experiences rapid growth during the third trimester and adolescence, with increasing cellular processes and white matter proliferation, continuing until age 30²⁸. Factors like cerebellar hemorrhage, tumors, and indirect damage (e.g., diaschisis) can lead to cerebellar volume loss. Studies on traumatic brain injury and animal models show cerebellar atrophy even without direct damage²⁹. The mechanism behind cerebellar atrophy can be attributed to three main reasons. Firstly, compression of the posterior fossa space by the swollen brainstem may limit normal neurodevelopment of cerebellum³⁰. Secondly, disruptions in anatomical pathways can cause cerebellar atrophy. Impairment of pontocerebellar fibers can obstruct axonal transport between the cerebellum and brainstem, damaging the cerebellar tract and deforming cerebellar neurons¹⁴. Thirdly, disruption of transsynaptic communication between pontine and cerebellar regions hinders fiber projection to Purkinje cells, leading to irreversible functional inactivation and long-term structural changes in the cerebellum³¹.

Our study represents a pioneering effort to link secondary cerebellar changes caused by brainstem tumors to behavioral patterns in pediatric patients. We utilized tOC as a quantitative metric to assess cerebellar atrophy at the individual level. The tOC has shown high stability and reliability in predicting neuroanatomical heterogeneity among patients with Alzheimer's disease²⁵. We found that heightened cerebellar atrophy corresponds to increased withdrawal behavior and social problems in children.

Using tOC as a metric for evaluating cerebellar health in individual patients could inform clinical decision-making. This discovery highlights the cerebellum's role in regulating social functions and provides evidence of its significance as a core brain region³².

Furthermore, our study found that negative deviations in the volume of cerebellar subregions were significantly associated with worse social behaviors. Specifically, the volume of posterior cerebellar regions like lobules X, IX, and VIII, exhibited a significant negative correlation with social problems. These findings are consistent with previous studies, reinforcing the notion that the posterior cerebellar lobes contribute to social functions³³. Moreover, the involvement of specific regions in the anterior cerebellar lobe, particularly lobules IV and V linked to the motor network, suggests that social functions are not limited to a single cerebellar area. This implies that social functions may be distributed across various areas of the cerebellum. For instance, functional MRI during social cognitive tasks has revealed activation in posterior cerebellar regions alongside the somatosensory motor network³². This connection highlights the complexity of cerebellar involvement in social functions. Furthermore, animal studies demonstrate that disrupted activity in anterior lobule IV/V leads to deficits in object recognition and social associative recognition tests, further supporting the cerebellum's role in cognitive and social processing³⁴.

A longstanding hypothesis in cerebellar research suggests that social dysfunction originates from damage in the vermis and posterior cerebellum³⁵. This aligns with the dichotomous theory of cerebellar functions, which distinguishes between sensorimotor and cognitive-affective regions based on anatomical connectivity patterns. The spinal cord, brainstem, and sensorimotor-associated cortical regions prominently connect with the anterior cerebellar lobe and lobule VIII³⁶. However, the latest perspective suggests that the cerebello-thalamo-cortical (CTC) and cerebello-ponto-cortical (CPC) tracts establish connections between the posterior cerebellum, Crus I/II, and the social regions located in the frontal

lobe³⁷. Consequently, researchers hypothesize that injury along this pathway manifests as social deficits, with damage around the CTC and CPC tracts predicting social and emotional disorders³⁸.

Moreover, it is important to note that the anterior and posterior cerebellar lobes, along with the vermis, show strong correlations with withdrawal behaviors. The anterior cerebellar lobe contributes most significantly to this association. This suggests that withdrawal behaviors may arise from dysfunction in the brain's social decision-making network³⁹. The cerebellum and brainstem are integral components of the social decision-making network, contributing primarily through their regulation of somatic motor nuclei⁴⁰. The present study suggests that the pathological withdrawal behaviors observed in patients may be attributed to severe atrophy of cerebellar motor nuclei. This finding corroborates numerous clinical observations indicating that children with lesions in the posterior fossa exhibit more complex and severe social problems, including withdrawal behaviors, attention deficit, irritability, pathological crying and laughing, and compression⁴¹. Importantly, extensive damage to the brainstem and cerebellar pedunculus results in more pronounced social dysfunction, with these behavioral disorders being profound and enduring.

This study creatively uses automated segmentation with the U-Net model to analyze cerebellar changes in brainstem tumor patients. Previous studies relied on basic measurements. Our approach provides precise quantification of cerebellar atrophy. This supports larger-scale clinical research. The use of a normative model reduces clinical and biological variability. This enhances the reliability of our findings. A key contribution is linking cerebellar damage from brainstem tumors to social behavior. While the impact of cerebellar injury on social functioning is known, neuroimaging evidence has been limited. Our study shows that damage near CPC and CTC tracts directly impairs social functions. This broadens the focus beyond the cerebellar vermis. The use of ridge regression offers valuable insights for large-scale neuroimaging studies in clinical settings.

However, this study has some limitations. Firstly, the normative model included only age and gender. It did not account for education or home environment, which might affect brain indices. Therefore, future models should include these factors. Secondly, the questionnaire focused mainly on social problems. It lacked depth in assessing social functions. A more specialized tool is needed. Thirdly, we found a correlation between cerebellar deformation and behavioral disturbances in pediatric patients. However, this does not establish causality.

This study reveals significant variability in how brainstem tumors affect the cerebellum. It introduces a reliable quantitative approach to assess this at the individual level. We analyzed deviations in cerebellar lobular volumes. Neuroanatomical outliers were linked to behavioral disorders, especially social and withdrawal behaviors. These findings emphasize the role of brainstem-cerebellar circuits in social behaviors and suggest that early recognition of cognitive and behavioral disorders may facilitate timely medical intervention. Protecting cerebellar-brainstem functional circuits could be crucial for preserving patient function and may inform surgical strategies, though further research is needed to validate these findings in clinical practice.

Data availability

The source data for Figs. 4, 5, 6 and Supplementary Figs 2 and 3 can be found in Supplementary Data 1. Clinical features analysis results are provided in Supplementary Materials, including cerebellar segmentation flowchart (Fig. S1) as well as Correlation between tOC and tumor volume (Fig. S2), behavioral results (Fig. S3), and effects of clinical features on behaviors (Table S1). Original data are available on reasonable request. Anonymous datasets not published within the article will be shared by the corresponding author on reasonable request by any qualified investigator.

Code availability

All processed codes used in this study is publicly available on GitHub at the following link: <https://github.com/heyan/cerebellum>⁴².

Received: 5 September 2024; Accepted: 17 March 2025;

Published online: 25 March 2025

References

- Boukaka, R. G. et al. Brainstem tumors in children: a monocentric series in the light of genetic and bio-molecular progress in pediatric neuro-oncology. *Front Pediatr.* **11**, 1193474 (2023).
- New, P. W. & Thomas, S. J. Cognitive impairments in the locked-in syndrome: A case report. *Archives of Physical Medicine and Rehabilitation.* **86**, 338–343 (2005).
- Omar, R. et al. The neuro-behavioural syndrome of brainstem disease. *Neurocase.* **13**, 452–465 (2007).
- Wolfe-Christensen, C., Mullins, L. L., Scott, J. G. & McNall-Knapp, R. Y. Persistent psychosocial problems in children who develop posterior fossa syndrome after medulloblastoma resection. *Pediatr Blood Cancer.* **49**, 723–726 (2007).
- Jia, H. et al. Brainstem tumors may increase the impairment of behavioral emotional cognition in children. *J Neurooncol.* **160**, 423–432 (2022).
- De Smet, H. J. et al. Long-term cognitive deficits following posterior fossa tumor resection: a neuropsychological and functional neuroimaging follow-up study. *Neuropsychology.* **23**, 694–704 (2009).
- Riva, D. & Giorgi, C. The cerebellum contributes to higher functions during development - Evidence from a series of children surgically treated for posterior fossa tumours. *Brain.* **123**, 1051–1054 (2000).
- Shah, A., Jhawar, S. S., Nunez, M., Goel, A. & Goel, A. Brainstem anatomy: A study on the basis of the pattern of fiber organization. *World Neurosurg.* **134**, e826–e846 (2020).
- Zhang, Z. Y., Liu, Z. Q., Qin, W., Chen, Y. W. & Liu, Z. J. Clinical and radiological features of Wallerian degeneration of the middle cerebellar peduncles secondary to pontine infarction. *China Med J (Engl).* **131**, 665–671 (2018).
- Schmahmann, J. D. & Sherman, J. C. Cerebellar cognitive affective syndrome. *Int Rev Neurobiol.* **41**, 433–440 (1997).
- Snider, R. S. & Maiti, A. Cerebellar contributions to the Papez circuit. *J. Neurosci. Res.* **2**, 133–146 (1976).
- Stoodley, C. J. & Limperopoulos, C. Structure-function relationships in the developing cerebellum: Evidence from early-life cerebellar injury and neurodevelopmental disorders. *Seminars in Fetal and Neonatal Medicine.* **21**, 356–364 (2016).
- Hansen, J. Y. et al. Integrating Brainstem and Cortical Functional Architectures. *Nature Neuroscience.* **27**, 2500–2511 (2024).
- Zhang, S., Ai, L., Chen, X. Z. & Wang, K. Radiological evaluation of infratentorial gangliogliomas in various anatomic locations of the cerebellum and brainstem. *Clin. Neuroradiol.* **27**, 319–327 (2017).
- Schmahmann, J. D. & Pandya, D. N. Course of the fiber pathways to pons from parasensory association areas in the rhesus monkey. *J Comp Neurol.* **326**, 159–179 (1992).
- Bushara, K. O. et al. Multiple tactile maps in the human cerebellum. *Neuroreport.* **12**, 2483–2486 (2001).
- Guell, X., Gabrieli, J. D. E. & Schmahmann, J. D. Triple representation of language, working memory, social and emotion processing in the cerebellum: convergent evidence from task and seed-based resting-state fMRI analyses in a single large cohort. *Neuroimage.* **172**, 437–449 (2018).
- D'aes, T. & Mariën, P. Cognitive and Affective Disturbances Following Focal Brainstem Lesions: A Review and Report of Three Cases. *The Cerebellum.* **14**, 317–340 (2014).
- Zuo, X. N. et al. An open science resource for establishing reliability and reproducibility in functional connectomics. *Scientific data.* **1**, 140049 (2014).
- Xi-Nian, Z. & Consortium, C. developing Chinese Color Nest Project (devCCNP) Lite. <https://doi.org/10.57760/sciencedb.07860> (2024).

21. Han, S., Carass, A., He, Y. & Prince, J. L. Automatic Cerebellum Anatomical Parcellation Using U - Net with Locally Constrained Optimization. *Neuroimage*. **218**, 116819 (2020).
22. Neo, W. S., Suzuki, T. & Kelleher, B. L. Structural validity of the Child Behavior Checklist (CBCL) for preschoolers with neurogenetic syndromes. *Res Dev Disabil*. **109**, 103834 (2021).
23. Johnson, W. E., Li, C. & Rabinovic, A. Adjusting Batch Effects in Microarray Expression Data Using Empirical Bayes Methods. *Biostatistics*. **8**, 118–127 (2007).
24. Marquand, A. F., Rezek, I., Buitelaar, J. & Beckmann, C. F. Understanding heterogeneity in clinical cohorts using normative models: beyond case-control studies. *Biol Psychiatry*. **80**, 552–561 (2016).
25. Verdi, S. et al. Revealing individual neuroanatomical heterogeneity in alzheimer disease using neuroanatomical normative modeling. *Neurology*. **100**, e2442–e2453 (2023).
26. Cui, Z. et al. Linking individual differences in personalized functional network topography to psychopathology in youth. *Biol Psychiatry*. **92**, 973–983 (2022).
27. Wei, Y. et al. Longitudinal gray matter atrophy and accompanied functional connectivity alterations in patients with pontine infarction. *Neurol Res*. **44**, 667–676 (2022).
28. Re, T. J. et al. High-angular resolution diffusion imaging tractography of cerebellar pathways from newborns to young adults. *Brain Behav*. **7**, e00589 (2017).
29. Spanos, G. K. et al. cerebellar atrophy after moderate-to-severe pediatric traumatic brain injury. *Am. J. Neuroradiol*. **28**, 537–542 (2007).
30. Larysz, D. et al. 271–274 (Springer Vienna).
31. Mah, S., deVeber, G., Wei, X. C., Liapounova, N. & Kirton, A. Cerebellar atrophy in childhood arterial ischemic stroke: acute diffusion MRI biomarkers. *Stroke*. **44**, 2468–2474 (2013).
32. Van Overwalle, F., Baetens, K., Marien, P. & Vandekerckhove, M. Social cognition and the cerebellum: a meta-analysis of over 350 fMRI studies. *Neuroimage*. **86**, 554–572 (2014).
33. Olson, I. R., Hoffman, L. J., Jobson, K. R., Popal, H. S. & Wang, Y. Little brain, little minds: The big role of the cerebellum in social development. *Dev. Cogn. Neurosci*. **60**, 101238 (2023).
34. Chao, O. Y., Zhang, H., Pathak, S. S., Huston, J. P. & Yang, Y. M. Functional Convergence of Motor and Social Processes in Lobule IV/ V of the Mouse Cerebellum. *Cerebellum*. **20**, 836–852 (2021).
35. Limperopoulos, C. et al. Does cerebellar injury in premature infants contribute to the high prevalence of long-term cognitive, learning, and behavioral disability in survivors? *Pediatrics*. **120**, 584–593 (2007).
36. Schmahmann, J. D., Guell, X., Stoodley, C. J. & Halko, M. A. The theory and neuroscience of cerebellar cognition. *Annu Rev Neurosci*. **42**, 337–364 (2019).
37. Carta, I., Chen, C. H., Schott, A. L., Dorizan, S. & Khodakhah, K. Cerebellar modulation of the reward circuitry and social behavior. *Science*. **363**, eaav0581 (2019).
38. Pitsika, M. & Tsitouras, V. Cerebellar mutism. *J Neurosurg-Pediatr*. **12**, 604–614 (2013).
39. Ike, K. G. O., de Boer, S. F., Buwalda, B. & Kas, M. J. H. Social Withdrawal: An Initially Adaptive Behavior That Becomes Maladaptive When Expressed Excessively. *Neurosci. Biobehav. Rev*. **116**, 251–267 (2020).
40. O'Connell, L. A. & Hofmann, H. A. The vertebrate mesolimbic reward system and social behavior network: a comparative synthesis. *J Comp Neurol*. **519**, 3599–3639 (2011).
41. Frazier, M. R. et al. A Missing Link in Affect Regulation: The Cerebellum. *Social Cognitive Affective Neuroscience*. **17**, 1068–1081 (2022).

42. Jia, H. Cerebellum analysis (Zenodo, 2025) <https://doi.org/10.5281/zenodo.15023957>.

Acknowledgements

We are grateful to the patients and their families for making brains available for research. We also express our gratitude to Bianka Rumi for her thorough proofreading of the entire text. We thank you for the support provided by the following fundings: STI2030-Major Projects (grant ID: 2021ZD0200201) and Beijing Municipal Public Welfare Development and Reform Pilot Project for Medical Research Institutes (grant ID: JYY202X-X).

Author contributions

L.Z. and L.F. conceived and designed the study. C.C., H.J., K.W., and X.W. contributed to the methodology. H.J., P.Z., M.Z., G.G., Y.M. and X.Y. contributed to the acquisition of data. H.J. and K.W. contributed to the statistical analysis. H.J. and K.W. contributed to drafting or critical revision of the manuscript. L.F., P.Z., and L.Z. acted as guarantor.

Competing interests

The authors declare no competing interests.

Ethical approval

Consent obtained directly from patients' parents.

Additional information

Supplementary information The online version contains supplementary material available at <https://doi.org/10.1038/s43856-025-00810-0>.

Correspondence and requests for materials should be addressed to Peng Zhang, Lingzhong Fan or Liwei Zhang.

Peer review information *Communications Medicine* thanks Shouliang Qi and Pierre-Aurélien Beuriat for their contribution to the peer review of this work. [A peer review file is available].

Reprints and permissions information is available at <http://www.nature.com/reprints>

Publisher's note Springer Nature remains neutral with regard to jurisdictional claims in published maps and institutional affiliations.

Open Access This article is licensed under a Creative Commons Attribution-NonCommercial-NoDerivatives 4.0 International License, which permits any non-commercial use, sharing, distribution and reproduction in any medium or format, as long as you give appropriate credit to the original author(s) and the source, provide a link to the Creative Commons licence, and indicate if you modified the licensed material. You do not have permission under this licence to share adapted material derived from this article or parts of it. The images or other third party material in this article are included in the article's Creative Commons licence, unless indicated otherwise in a credit line to the material. If material is not included in the article's Creative Commons licence and your intended use is not permitted by statutory regulation or exceeds the permitted use, you will need to obtain permission directly from the copyright holder. To view a copy of this licence, visit <http://creativecommons.org/licenses/by-nc-nd/4.0/>.

© The Author(s) 2025